PLANETARY SCIENCE

MAVEN observations of the response of Mars to an interplanetary coronal mass ejection

B. M. Jakosky,[1]* J. M. Grebowsky,[2] J. G. Luhmann,[3] J. Connerney,[2] F. Eparvier,[1] R. Ergun,[1] J. Halekas,[4] D. Larson,[3] P. Mahaffy,[2] J. McFadden,[3] D. F. Mitchell,[3] N. Schneider,[1] R. Zurek,[5] S. Bougher,[6] D. Brain,[1] Y. J. Ma,[7] C. Mazelle,[8,9] L. Andersson,[1] D. Andrews,[10] D. Baird,[11] D. Baker,[1] J. M. Bell,[21] M. Benna,[2] M. Chaffin,[1] P. Chamberlin,[2] Y.-Y. Chaufray,[12] J. Clarke,[13] G. Collinson,[2] M. Combi,[6] F. Crary,[1] T. Cravens,[14] M. Crismani,[1] S. Curry,[3] D. Curtis,[3] J. Deighan,[1] G. Delory,[3] R. Dewey,[1] G. DiBraccio,[2] C. Dong,[6] Y. Dong,[1] P. Dunn,[3] M. Elrod,[2] S. England,[3] A. Eriksson,[10] J. Espley,[2] S. Evans,[15] X. Fang,[1] M. Fillingim,[3] K. Fortier,[1] C. M. Fowler,[1] J. Fox,[16] H. Gröller,[17] S. Guzewich,[2] T. Hara,[3] Y. Harada,[3] G. Holsclaw,[1] S. K. Jain,[1] R. Jolitz,[3] F. Leblanc,[12] C. O. Lee,[3] Y. Lee,[6] F. Lefevre,[12] R. Lillis,[3] R. Livi,[3] D. Lo,[17] M. Mayyasi,[13] W. McClintock,[1] T. McEnulty,[1] R. Modolo,[12] F. Montmessin,[12] M. Morooka,[1] A. Nagy,[6] K. Olsen,[6] W. Peterson,[1] A. Rahmati,[14] S. Ruhunusiri,[4] C. T. Russell,[7] S. Sakai,[14] J.-A. Sauvaud,[8,9] K. Seki,[18] M. Steckiewicz,[8,9] M. Stevens,[19] A. I. F. Stewart,[1] A. Stiepen,[1] S. Stone,[17] V. Tenishev,[6] E. Thiemann,[1] R. Tolson,[20] D. Toublanc,[8,9] M. Vogt,[13] T. Weber,[1] P. Withers,[13] T. Woods,[1] R. Yelle[17]

Coupling between the lower and upper atmosphere, combined with loss of gas from the upper atmosphere to space, likely contributed to the thin, cold, dry atmosphere of modern Mars. To help understand ongoing ion loss to space, the Mars Atmosphere and Volatile Evolution (MAVEN) spacecraft made comprehensive measurements of the Mars upper atmosphere, ionosphere, and interactions with the Sun and solar wind during an interplanetary coronal mass ejection impact in March 2015. Responses include changes in the bow shock and magnetosheath, formation of widespread diffuse aurora, and enhancement of pick-up ions. Observations and models both show an enhancement in escape rate of ions to space during the event. Ion loss during solar events early in Mars history may have been a major contributor to the long-term evolution of the Mars atmosphere.

Quantifying the role that escape of gas to space played throughout martian history will help to determine whether it was an important mechanism for driving the climate change observed in the geological record (*1*, *2*). Determining the effects that discrete solar storms have had on the structure of the upper atmosphere, ionosphere, and magnetosphere, and on the loss rate to space, is an important component of this, owing to the increased occurrence of storms in early martian history and their potential contributions to the total loss.

The Mars Atmosphere and Volatile Evolution (MAVEN) mission to Mars was designed to study the upper atmosphere, ionosphere, and magnetosphere of Mars, the response to solar and solar-wind input, and the ability of atmospheric molecules and atoms to escape to space (*3*). MAVEN was launched on 18 November 2013, and went into orbit around Mars on 21 September 2014. After a 2-month commissioning phase, it began its one-Earth-year primary science mission on 16 November 2014. MAVEN is in an elliptical orbit with periapsis altitude of ~150 km and apoapsis altitude of ~6200 km. This orbit allows a combination of in situ measurements throughout the entire region of interest and remote-sensing measurements that provide quasi-global coverage. The nine science instruments provide a combination of measurements of the solar and solar-wind energetic input into the upper atmosphere, the composition and structure of the upper atmosphere and ionosphere, the topology of the interactions of the solar wind with the planet, and the composition and energetics of atomic and molecular ions interacting with and escaping from the system (*3*, *4*).

We report here on observations from MAVEN that show the integrated effects of an interplanetary coronal mass ejection (ICME) with the planet, the consequences for the upper atmosphere, and the impact on escape to space. We both present the observations made by MAVEN of the ICME and Mars atmospheric response, and use the observations to validate a global model of the martian atmosphere interaction with the solar wind during the ICME. The model is then used to estimate the global response of the system, which MAVEN samples only locally during the event. These observations complement studies of the structure of the upper atmosphere and ionosphere and the overall behavior of the martian system, along with the initial look at the chain of events from energetic drivers to response of the upper atmosphere and then leading to escape to space (*4*–*7*).

Energetic inputs into the system

MAVEN has been making observations nearly continuously since November 2014. The strongest solar event observed to date occurred on 8 March 2015. MAVEN measurements during the entire time period from 25 February to 13 March 2015 exhibited disturbed interplanetary conditions, as shown in Fig. 1. The solar irradiance time series from the perspective of Mars (Fig. 1, top panel) shows the flare activity detected by the MAVEN extreme ultraviolet (EUV) detector. The flare event (F4) occurring on 6 March ~05:00 UT was likely associated with the major interplanetary disturbance of this period. Major flares are often related to eruptions of coronal material known as coronal mass ejections (CMEs, best known for causing geomagnetic storms at Earth) (*8*). White light coronagraph images from the Solar Heliospheric Observatory (SOHO) showed that multiple CMEs erupted in the general direction of Mars during this time.

We used orbital ephemerides and Magnetomer (MAG) (*9*) and Solar Wind Ion Analyzer (SWIA) (*10*) measurements to select periods during which we had unambiguous measurements of the upstream solar wind outside of the martian bow shock and foreshock. The solar-wind density, velocity, and interplanetary magnetic field (IMF) were averaged over the upstream interval, for each MAVEN orbit for which they could be determined. The most disturbed period analyzed here spanned about three ~4.5-hour MAVEN orbits.

The upstream solar-wind data set shows four major density enhancements (labeled S1 to S4) associated with a series of ICMEs. During the last of these events (S4) on 8 March, the solar wind reached a peak flow speed of 825 km/s, with a corresponding peak ram pressure of 15 nPa, and magnetic-field strength of ~20 nT, all the highest values observed by MAVEN to date. For comparison, the peak pressure observed at Mars during the Halloween 2003 ICME event was ~33 nT, and the average pressure during this period was ~7 nPa (*11*); the event reported here is one of the strongest ever observed at Mars. The average upstream solar

[1]University of Colorado, Boulder, CO, USA. [2]NASA/Goddard Space Flight Center, Greenbelt, MD, USA. [3]University of California at Berkeley, Berkeley, CA, USA. [4]University of Iowa, Iowa City, IA, USA. [5]Jet Propulsion Laboratory, California Institute of Technology, Pasadena, CA, USA. [6]University of Michigan, Ann Arbor, MI, USA. [7]University of California at Los Angeles, Los Angeles, CA, USA. [8]CNRS–Institut de Recherche en Astrophysique et Planétologie (IRAP), Toulouse, France. [9]University Paul Sabatier, Toulouse, France. [10]Swedish Institute of Space Physics, Uppsala, Sweden. [11]NASA/Johnson Space Center, Houston, TX, USA. [12]Laboratoire atmosphères, milieux et observations spatiales (LATMOS)–CNRS, Paris, France. [13]Boston University, Boston, MA, USA. [14]University of Kansas, Lawrence, KS, USA. [15]Computational Physics, Inc., Boulder, CO, USA. [16]Wright State University, Dayton, OH, USA. [17]University of Arizona, Tucson, AZ, USA. [18]Nagoya University, Nagoya, Japan. [19]Naval Research Laboratory, Washington, DC, USA. [20]North Carolina State University, Raleigh, NC, USA. [21]National Institute of Aerospace, Hampton, VA, USA.
*Corresponding author. E-mail: bruce.jakosky@lasp.colorado.edu

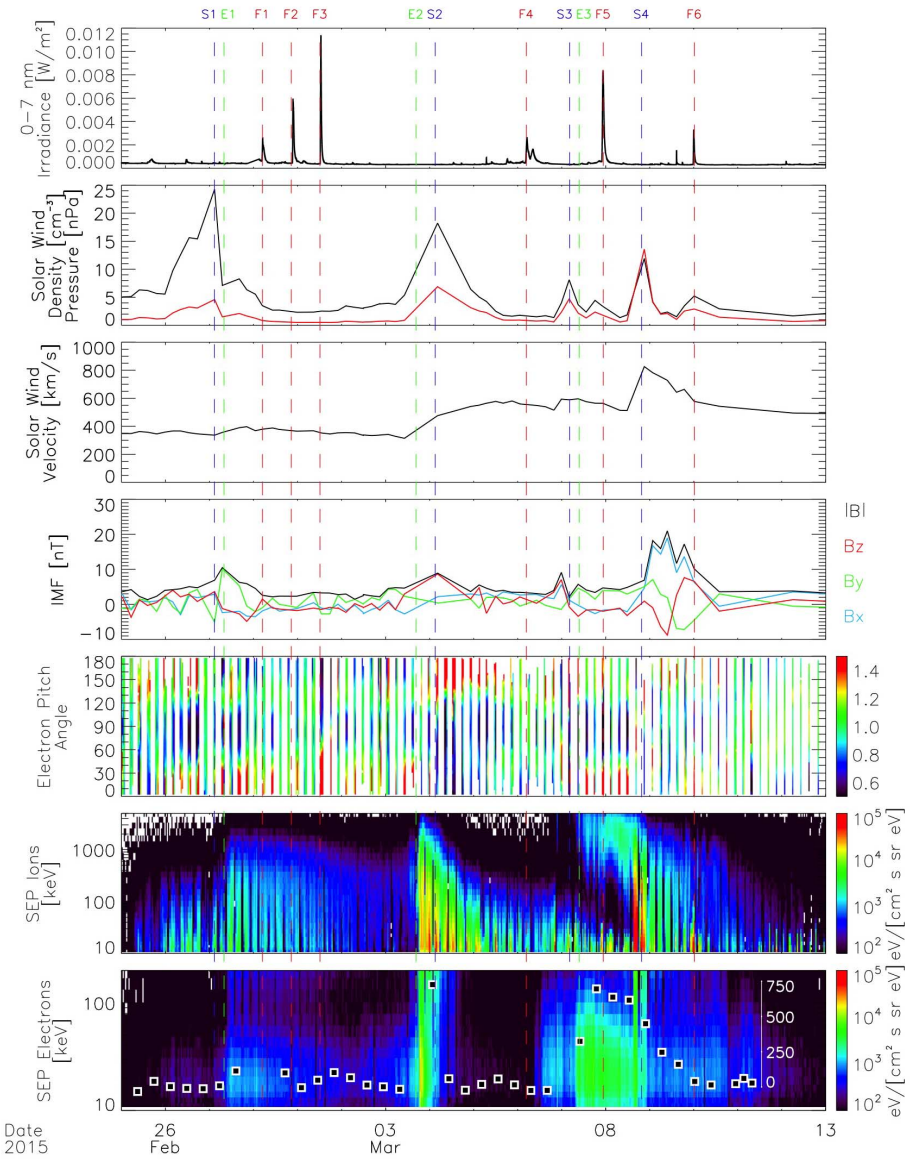

Fig. 1. Energy inputs to the martian system. The seven panels show flare irradiance from EUVM, solar-wind density (black) and ram pressure (red), velocity, and interplanetary magnetic field computed from SWIA and MAG data averaged over the portion of the orbit when the spacecraft was upstream from the bow shock, electron pitch-angle distributions at 110 to 140 eV from SWEA, and energetic ion and electron differential energy flux spectra from SEP. The intensities of CO_2^+ UV doublet auroral emission at 289 nm from the Mars nightside are plotted over the energetic electrons, using the inset scale; values below 50 to 100 Rayleighs are attributed to instrumental noise.

wind values measured by MAVEN from late November 2014 to late March 2015 were ~1 nPa for the ram pressure and 4 nT for the magnetic-field strength. The detailed MAG data from within the induced magnetosphere (discussed below) indicates that at ~15:20 UT 8 March, a strong magnetic rotation and compression associated with the arrival of the major ICME of the interval (event S4) were seen. The IMF returned to a more typical level within 48 hours after this signature. Major ICME events often have durations of up to a few days.

The Solar Wind Electron Analyzer (SWEA) (*12*) instrument measured suprathermal electron pitch-angle distributions (Fig. 1, fourth panel) upstream of the Mars bow shock. These reveal the magnetic topology associated with this series of events. The topology leading up to the final series of events (S3, S4) is complex, with electron beaming reversals and counterstreaming, suggesting that magnetically "closed" topologies are present almost every orbit. Such interplanetary field topologies, which are characteristic of ICME drivers and complex space-weather events, also affect the solar-wind interaction with Mars by altering the details of external field reconnection with the Mars crustal fields.

Solar energetic particle (SEP) events (*13*) (E1 to E3) were seen in conjunction with the multiple ICME passages, as shown in Fig. 1 (last two panels). The highest SEP ion fluxes at lower energies (<1 MeV) peaked around the ICME shock arrival times (S2 and S4), consistent with energetic storm particle (ESP) enhancements that occur when an ICME makes a direct strike. The most energetic ions (>1 MeV) in the strong event (E3) reached Mars at ~08:00 UT 7 March, ahead of the ICME disturbance (S4). This is the classical velocity dispersion, where the most energetic ions arrive first, at least a day before the plasma and field disturbance. The SEP ions gradually diminished in intensity throughout the rest of the ICME disturbance. SEP ion energy deposition in the Mars atmosphere peaked for ICME events S2 and S4, the latter being stronger. The largest energy fluxes occurred below ~300 keV, where most energy is deposited between 100- and 140-km altitude (*14*) and should affect strongly the thermospheric reservoir from which atmospheric escape occurs (*15*). The observed SEP electrons (bottom panel), which arrived early with the most-energetic ions, show a spread in energy at the ICME shock arrival on 8 March and a diminished flux soon after the shock passage.

We used the Wang-Sheeley-Arge (WSA)–ENLIL+Cone model to numerically simulate the interplanetary solar-wind conditions and provide a global heliospheric context for these events at Mars (*16*). Based on the simulation, the 8 March ICME impact of Mars was composed of two individual transients that merged en route to the planet. The first ICME was injected into the inner boundary of the ENLIL solar wind model at 04:49 UT 6 March with an initial radial speed of

900 km/s, whereas the second ICME was injected at 07:12 UT 6 March with a faster speed of 1500 km/s. The southern part of the second ICME interacted with and overtook the first ICME to produce a merged ICME. The model predicted the eastern flank of the merged structure to strike Mars at ~11:40 UT 8 March. Interestingly, the active region that triggered the Mars-directed ICMEs subsequently rotated toward Earth and launched an ICME, to produce one of the strongest geomagnetic storms of the current solar cycle (*17*).

Response of the system

MAVEN observations show that the ICME impact on 8 March 2015 dramatically altered the overall morphology and dynamics of the magnetosphere, affected the ionosphere, and induced auroral emissions from the neutral atmosphere.

Prior to the ICME, SWIA (*10*) measured a solar-wind proton density of 1.8 cm^{-3}, an alpha-particle density of 0.1 cm^{-3}, and flow speed of 505 km/s, corresponding to a ram pressure of 0.9 nPa. MAG (*9*) measured a typical IMF magnitude of ~5 nT. After the passage of the ICME shock, the upstream proton density rose to as high as 11 cm^{-3}, the alpha density to 0.6 cm^{-3}, and the flow speed to 820 km/s, with a ram pressure of 15 nPa, the highest encountered to date during the MAVEN mission. The IMF increased to 14 nT and in succeeding days rose to as high as 20 nT, also the highest value seen so far.

Using these measurements as inputs, we calculated three steady-state cases with a multispecies magnetohydrodynamic (MHD) model (*18*) to provide global context for the observations. The solar-wind conditions are set corresponding to before the ICME arrival (case 1), shortly after the arrival (case 2), and during the later time of the ICME, when the solar-wind dynamic pressure was intensified (case 3). Data-model comparisons are shown in Fig. 2. The orbit prior to arrival of the ICME, with apoapsis near 11:10 UT and periapsis at 13:23 UT, provides a baseline. Given the nominal IMF magnitude and plasma density, but moderately high Mach number of the flow, the observed and modeled magnetospheric boundaries are both asymmetric. The quasi-parallel bow-shock crossing on the outbound portion of the apoapsis segment occurred slightly earlier than expected from its average location (*19*), but the inbound boundaries were close to their nominal positions. MAVEN observed only minor crustal magnetic fields (*20*) of ~10 nT near periapsis, a total magnetic field of ~50 nT in the ionosphere, and few fluctuations.

During the succeeding apoapsis segment, MAVEN encountered extremely unusual plasma, with 10% alpha-particle abundance, a flow speed of 825 km/s with a 150 km/s off-axis component, and a high proton temperature of 130 eV, suggesting

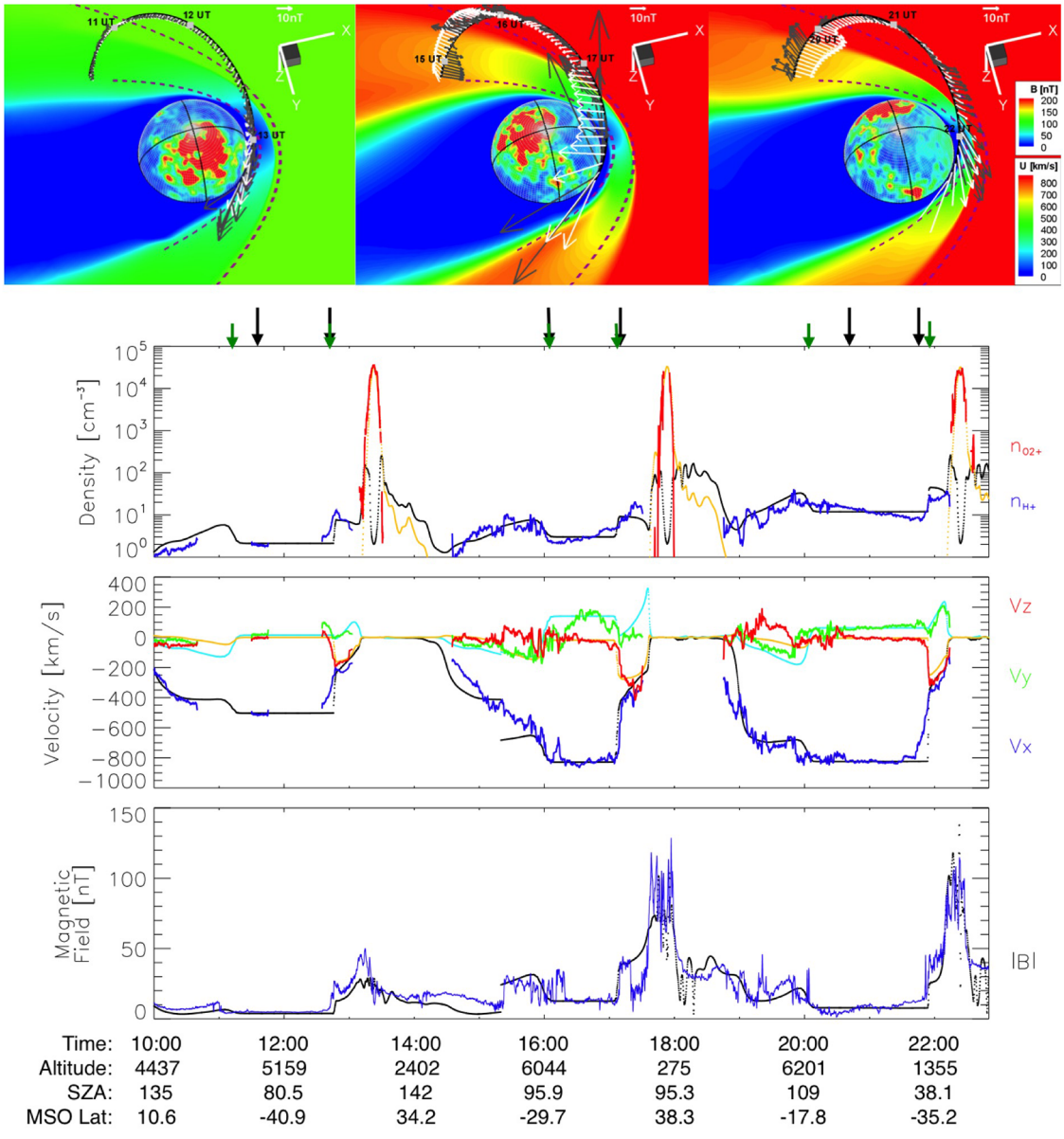

Fig. 2. The response of the martian magnetosphere to the passage of an ICME. The top panel shows predicted magnetospheric structure for three orbits, based on MHD runs utilizing upstream solar-wind conditions. The color contours show plasma flow speed in the equatorial plane (from the south). Black lines indicate the MAVEN orbit, black arrows show measured magnetic fields, and white arrows show model fields. The three-dimensional sphere represents the inner model boundary at 100-km altitude, with colors indicating the crustal magnetic field strength at the time of periapsis. The black dashed lines show nominal ionosphere-magnetosphere boundary and bow shock positions. The bottom three panels show MAG, SWIA, STATIC, and NGIMS (Neutral Gas and Ion Mass Spectrometer) observations (solid lines), with MHD results for comparison (dotted lines). Green and black arrows mark the observed and nominal bow shock locations, respectively.

that MAVEN encountered the sheath region trailing the ICME shock. The combination of high ram pressure and low Mach number conspired to produce boundaries near their normal position, but we observed multiple shock crossings and large magnetic fluctuations during this time period, implying a highly dynamic interaction. Commensurate with the high ram pressure, the average draped field inside the magnetosphere increased to ~90 nT, with a maximum of 130 nT during periapsis. The MHD model matches the overall magnetospheric structure during this period, but the time-stationary model cannot capture the observed variability and fluctuations in magnetic-field direction.

The magnetospheric effects continued and intensified in the succeeding orbit. The magnetic field exhibited large fluctuations, and the draped field remained at ~90 nT. The solar wind flow remained >800 km/s for ~7 hours, and the density increased, producing a solar-wind ram pressure more than an order of magnitude larger than typically observed and resulting in substantial deformation of the bow shock and compression of the entire magnetosphere. The MHD model, which matches the data well during this period, shows these effects globally.

On smaller scales, MAVEN observed sharp isolated magnetic-field enhancements in the martian magnetosheath just after the ICME shock arrival on 8 March. The enhancements are associated with magnetic-field rotations characteristic of magnetic flux ropes (*21*), which are observed to occur in the martian ionosphere and downstream from crustal magnetic fields (*22*, *23*). Suprathermal and Thermal Ion Composition (STATIC) measurements indicate that heavy (i.e., planetary) ions are present in the flux-rope structures, with energies of a few kilo–electron volts. The presence of heavy planetary ions collocated with flux ropes at the 5000-km altitude of the observed structures allows us to infer that the flux ropes formed in the vicinity of the ionosphere. The magnetic-field amplitudes in the flux ropes exceeded 80 nT, which is a few times larger than the typical detached flux ropes seen during nominal solar-wind conditions. Strong-field detached flux ropes observed at high altitudes are unique in the MAVEN observations to date. Moreover, the velocity of the detached flux ropes is estimated to be much faster than usual by a factor of approximately 10, under the assumption that these structures are in magneto-hydrostatic equilibrium (*24*).

The March ICME events also affected the upper atmosphere. MAVEN's Imaging Ultraviolet Spectrograph (IUVS) detected diffuse auroral emissions during the ICME events similar to those observed in December 2014 (*6*). IUVS is a remote-sensing instrument designed to map UV atmospheric emissions with altitude and across the planetary disk (*25*). The most sensitive mode for detection of auroral emission uses limb scans taken near periapsis on Mars' nightside. The vast majority of nightside limb scans show no atmospheric emissions apart from the ubiquitous hydrogen Lyman alpha (*26*) and occasional NO band emissions.

Observations spanning 22 min near periapsis were obtained on alternating orbits at ~9-hour intervals during the period encompassing the ICME. Figure 1 (bottom panel) shows the observed timeline for auroral emission from Mars' nightside during this period. The figure plots emission from the CO_2^+ UV doublet at 289 nm. Fainter emission was also detected from the CO Cameron bands. Both emissions are generated by particle impact on CO_2, which causes ionization, dissociation, and excitation. These emissions have been well studied on Mars' dayside, where they are excited by solar EUV radiation and resulting photoelectrons, and have been observed since the Mariner missions (*27*). The same emissions were observed on the Mars nightside in discrete aurora detected by the SPICAM (Spectroscopy for Investigation of Characteristics of the Atmosphere of Mars) instrument on Mars Express near crustal magnetic fields (*28*), and were seen previously by MAVEN in widespread diffuse aurora far from crustal fields and associated with a solar event (*6*).

IUVS detected three separate episodes of substantial auroral emission. The first occurred on 27 to 28 February and the second in a single orbit on 4 March. On 7 March, emission was observed to rise, peak, and fall over ~50 hours; no data were taken on the orbits immediately preceding the rise or following the decline. Although the seven detections in the third event are limited to ~20-min periods separated by ~9 hours, the repeated detections and relatively smooth variation suggest that it was a widespread, sustained event. The event spanned more than one Mars rotation, indicating that geographic control of this type of auroral emission is weak or nonexistent.

Substantial ion energization and enhancement resulting from the disturbed conditions were observed by SWIA, STATIC, and SEP during the 8 March event, as seen in measurements from a single MAVEN orbit shown in Fig. 3, after the arrival of the ICME shock. Although pickup ions are evident during the entire disturbed period subsequent to the maxima in IMF strength and ram pressure around 14:00 UT, we focus on the orbit spanning ~18:00 to 22:00 on 8 March.

The SWIA instrument (*7*) recorded strong pickup ion enhancements during this orbit (Fig. 3C). The solar wind is evident at high altitudes as a continuous flux of protons with energy per charge of 2 to 5 keV/q and alpha particles with energy per charge of 6 to 9 keV/q. Intermittent periods of higher-energy ion flux (~10 keV and above) appear at high altitudes. The black trace in Fig. 3C illustrates the predicted energy of pickup ions originating from any point directly sunward from the martian subsolar point (*29*) and accelerated entirely by the measured local $\mathbf{V} \times \mathbf{B}$ electric field. The predicted pickup ion energies have good agreement with the observations and correspond to periods where high-energy ion fluxes are observed. This agreement suggests that planetary ions were accelerated to high energies by the local convection electric field.

The STATIC (*30*) instrument also measures ions and can discriminate mass. Figure 3, D and E, show the observed energies [for mass >9 atomic mass units (amu)] and masses of ions during this orbit. Near periapsis, both O_2^+ and CO_2^+ are evident, and as the spacecraft altitude increases, the flux of massive CO_2^+ molecules decreases rapidly, and O^+ fluxes increase. Also present is a probable signature of He^+, most likely produced from charge exchange between solar-wind helium and planetary neutrals, as recently observed by Rosetta (*31*). This population also can be observed during quiet times, but is intensified during this period owing to the high solar-wind flux. Heavy-ion observations at high altitudes are complicated by the substantial solar-wind proton fluxes during the ICME. Internally scattered protons can contaminate higher-mass channels and have been removed via a background subtraction algorithm. Even though the background subtraction errs on the side of subtracting too many counts at high masses, fluxes of high-mass species are distinguishable periodically all the way up to apoapsis, often at energies higher than the predicted pickup ion energy shown in Fig. 3C. A closer look at the period near apoapsis (Fig. 3F) reveals that O^+, O_2^+, and CO_2^+ are all present at energies substantially greater than the solar-wind energy and have been stripped away from the planet.

At even higher energies, the SEP instrument (*13*) detected pick-up oxygen ions that had been produced upstream in the neutral oxygen corona and then accelerated toward Mars; these pick-up ions had energies above ~70 keV. The maximum oxygen pickup ion energy is given by $E_{max} = 2\, m_o\, U_{sw}^2\, \sin^2\theta_{UB}$, where m_o is the mass of atomic oxygen, U_{sw} is the solar-wind speed, and θ_{UB} is the angle between the solar wind and the IMF; after the 8 March ICME arrival, solar-wind velocities in excess of 800 km/s enable acceleration of pickup oxygen to energies as high as 210 keV. Following the method of (*32*), pickup oxygen fluxes are simulated for the first MAVEN apoapsis after the ICME arrival (the orbit prior to the one shown in Fig. 3, A to E, because of more favorable observing geometry during that orbit), and the agreement between the SEP measured and modeled fluxes confirms detection of O^+ by SEP. Figure 3G illustrates MAVEN data for a 45-min time period after 16:20 UT, when MAVEN was in the undisturbed upstream solar wind. For most of this time period, θ_{UB} was ~50°, giving an E_{max} of ~120 keV. The elevated background noise in the SEP data is due to energetic particles associated with the ICME. Oxygen pickup ions detected by SEP during the ICME event have the highest energies observed since MAVEN's arrival at Mars.

Loss to space

We can compare planetary ion fluxes during the ICME event to those observed over many months as a means for assessing the likely impact of the ICME on atmospheric escape rates. In addition, we can calculate the escape rate using MHD models of the interaction of the solar wind with the planet and using measured solar-wind conditions as model inputs. Both show a substantial enhancement in the escape rate during the ICME event.

To determine the measured escape rate, we use STATIC (*30*) observations of heavy-ion fluxes

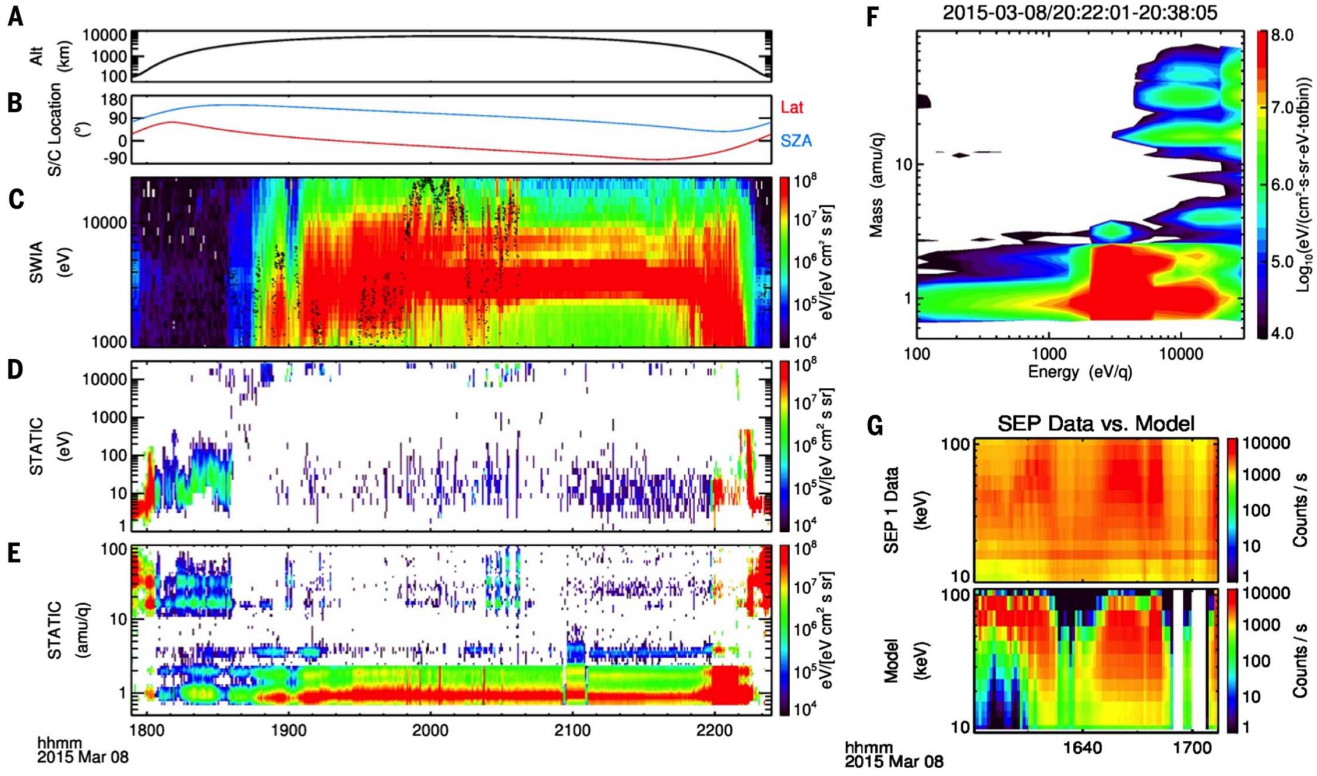

Fig. 3. MAVEN charged-particle observations reveal the presence of pick-up ions during the 8 March 2015 ICME. Observations from a single orbit are shown in (A) to (D). (**A**) Spacecraft altitude. (**B**) Spacecraft location given as latitude and solar zenith angle. (**C**) SWIA observations of ion energy fluxes as a function of energy, with the predicted energy of subsolar pickup ions given by the black trace. (**D**) STATIC observations of high-mass (>9 amu/q) ion energy fluxes as a function of energy. (**E**) STATIC observations of ion energy fluxes as a function of ion mass. (**F**) STATIC observations near periapsis of ion energy fluxes as a function of energy and mass simultaneously, showing both the low-mass solar wind and high-energy, high-mass pickup ions. (**G**) Observed and modeled SEP spectra for ~40 min during the beginning of the ICME passage, on the orbit prior to the one shown in (A) to (D).

during time periods when the spacecraft occupied altitudes between 0.25 and 0.45 planetary radii. At these altitudes, observations cover a large fraction of the sphere enclosing Mars, and the measurements provide a good estimate of the total escape. MAG and SWIA measurements of the IMF and solar-wind velocity, respectively, were used to rotate the spacecraft position into a Mars-Solar-Electric field (MSE) coordinate system, with MSE-x antiparallel to the incident solar-wind flow, MSE-y parallel to the IMF direction projected into the plane perpendicular to the flow, and MSE-z in the direction of the convection electric field given by $-\mathbf{V} \times \mathbf{B}$. Such a coordinate system is frequently used to organize escaping planetary ion fluxes [e.g., (*33*)], which should be strongly influenced by the electric field in the solar wind. Individual observations recorded when the instrument was in "pickup mode" (32 energy bins, 8 mass bins, and 64 look directions) were separated so that ion flux toward and away from the planet were tracked separately. We limit ourselves to energies greater than 25 eV, as the MAVEN data have not been corrected yet for the effects of spacecraft electric potential that can significantly influence the low-energy measurements. Inclusion of low-energy particles will increase both the reported fluxes and escape rates, with the consequence that we present lower limits here. Previous studies (*34*) have shown that reported escape rates depend at least partly on the energy range of ions being considered.

A comparison of fluxes during the ICME event (2015-03-08/16:00 to 2015-03-09/12:00) to median fluxes over a period of approximately 4 months is shown in Fig. 4. Because of uncertainties in the direction of the electric field during the turbulent ICME event, we show the results as a function of solar zenith angle. This comparison is valid independent of the electric-field direction. Most notable is the strong flux of planetary ions away from the planet on the dayside during the ICME, in a region usually dominated by the flow of ions toward the planet. These fluxes are among the strongest observed in this region during the entire mission. Nightside regions sampled during the ICME have fluxes more characteristic for their location, or even lower than is typical.

We cannot reliably provide a global escape rate during the ICME event based on these sparse observations alone, owing to the limited coverage over a short time period. However, it appears that escape rates on the nightside of the planet remained at values during the ICME that were similar to values at other times, and that dayside escape rates of planetary ions were enhanced considerably. Previous measurements of ion escape rates during ICMEs have been reported (*35*) and suggest that total escape rates can be 10 to 100 times greater during solar storm events.

The good agreement described earlier between the MHD model and MAVEN observations during the ICME event gives us confidence to use the model to infer the variations of the ion loss rate during the ICME passage. The integrated ion loss rates are listed in Table 1 using model results of the same three cases described earlier. Before the ICME arrival, the model predicted that the integrated escape rate was of the order of 1.5×10^{24}/s, dominated by O_2^+ ions. As the flow speed of the solar wind increased to more than 800 km/s shortly after the ICME arrival, the solar-wind dynamic pressure was about four times enhanced, and the model predicted that the total ion escape rate would increase to ~10^{25}/s, which is seven times larger than the ion loss rate during nominal conditions. When the solar-wind density and velocity were both enhanced, the corresponding solar-wind dynamic pressure increased to ~15 times, and the escape rate for case 3 reached 3×10^{25}/s, more than an order of magnitude enhancement. The major ions lost to space changed from O_2^+ (in both case 1 and 2) to O^+ ions in case 3. This model prediction is consistent with measurements made by STATIC, which detected a large increase in O^+ ion fluxes during the orbits after the ICME arrival. This increase is likely caused by enhancement of O^+ ion production through augmented electron-impact ionization and charge-exchange reactions

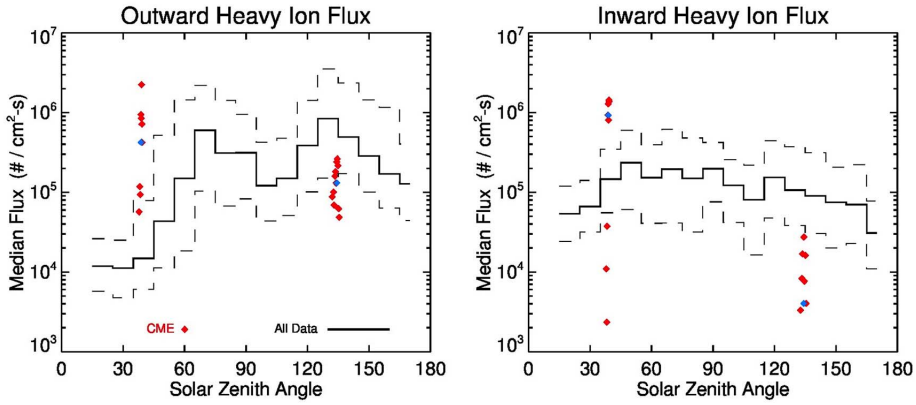

Fig. 4. Comparison of loss during ICME with integrated loss through the mission to date. Planetary heavy ion fluxes (>9 amu) measured by STATIC during the ICME event (red, with median value shown in blue) are shown in comparison to median and first/fourth quartile ion fluxes measured over a ~4 month period (gray traces). Fluxes are evaluated in a spherical shell around Mars from 1.25 to 1.45 R_M (radius of Mars), and the position of MAVEN is rotated into a coordinate system aligned with the solar wind electric field. During the ICME, strong outward flux is observed in regions of typically inward flow.

Table 1. Ion loss rates calculated by the MHD model for the three cases corresponding to three different stages of the ICME. *P*sw is the solar-wind pressure for the model run.

	P_{SW} (nPa)	O^+ (s^{-1})	O_2^+ (s^{-1})	CO_2^+ (s^{-1})	Total (s^{-1})	Total (kg/s)
Case 1	0.9	6.4×10^{23}	7.7×10^{23}	4.9×10^{22}	1.46×10^{24}	0.06
Case 2	3.4	2.6×10^{24}	7.6×10^{24}	3.3×10^{23}	1.06×10^{25}	0.50
Case 3	13.4	1.96×10^{25}	1.32×10^{25}	6.3×10^{23}	3.34×10^{25}	1.27

between solar-wind protons and neutral oxygen atoms, resulting from the intense electron and proton fluxes in the ICME.

Similarly, a multifluid MHD model (*36*, *37*) predicted more than an order-of-magnitude enhancement of the ion loss rates during extreme solar-wind conditions associated with the ICME. The multifluid model results were also used to examine the relative importance of the two major ion loss channels from the planet—energetic-ion loss through the dayside polar plume and cold-ion loss through the nightside plasma-wake region. Escape of ions from the dayside polar plume could be as much as ~30% prior to the ICME arrival. When solar-wind dynamic pressure was drastically intensified, the ratio of escape rates from the polar plume reduced to ~10%, and the cold ions escaping from the plasma wake made up most of the ion loss from the planet.

Both the observations and the model results suggest there are substantial enhancements in the ion loss rates during ICME events. The agreement of the models with the observations reinforces the interpretation and allows a global estimate of the increase of about an order of magnitude to be made. The ion loss reported here is only one means by which gas can be removed from the atmosphere. Particles can also be removed to space as neutrals. Neutral escape may prove to be the dominant loss channel, but observations are more difficult to interpret. These ion loss enhancements can thus be considered a lower limit on the escape enhancement.

The results obtained by MAVEN for this strong ICME event can be compared with previous measurements of ion escape at Mars during disturbed periods. These include case studies (*35*, *38*), and statistical studies during CIR events, solar maximum, and solar minimum periods (*39*–*42*). The compression of the magnetosphere in response to high dynamic pressure is consistent with observations of disturbed conditions presented in the studies cited above. Nearly all of these studies also suggest an increase in ion escape rates during disturbed periods, but differ in the degree to which they change. Our results are consistent with the case study presented by Futaana *et al.* (*35*), which estimated an order-of-magnitude increase in planetary ion fluxes (and thus escape) in response to an ICME event observed by Mars Express. By contrast, our results appear to be inconsistent with a recent statistical reanalysis of Mars Express observations that shows a decrease in escape rates in response to increased solar-wind density (*41*). Though the reason for the discrepancies between previous studies can include differences in data selection and analysis method, it seems likely that different events and different kinds of events induce responses of different magnitude at Mars. Constraining how ICME events influence ion escape is an important component for understanding escape rates from early Mars.

Conclusions and future observations

MAVEN observations show a major impact of the ICME observed in March 2015. The effects through the entire upper-atmosphere–ionosphere–magnetosphere system produced substantially disturbed conditions and appeared to have a major impact on the instantaneous rates of loss of ions to space. Given the likely prevalence of ICME-like conditions earlier in solar-system history (*43*), it is possible that ion escape rates at that time were dominated by storm events. As these early periods may have been the dominant times at which the martian atmosphere experienced loss, the inferred climate change on Mars may have been driven to a large extent by these solar storms.

The MAVEN spacecraft is continuing to collect observations. These ongoing observations will fill in the three-dimensional space surrounding Mars and allow us to better understand the processes occurring in the upper atmosphere and ionosphere and to observe the response to changing external forcing in the form of the changing solar EUV, solar wind, and solar storms. Ongoing observations also will show the response to the changing martian seasons, eventually allowing coverage of a full Mars year and beyond.

REFERENCES AND NOTES

1. M. H. Carr, Water on Mars. *Nature* **326**, 30–35 (1987). doi: 10.1038/326030a0
2. D. J. Des Marais, B. M. Jakosky, B. M. Hynek, Astrobiological implications of Mars surface composition and properties, in *The Martian Surface: Composition, Mineralogy, and Physical Properties*, J. F. Bell III, Ed. (Cambridge Univ. Press, Cambridge, 2008), 599–623.
3. B. M. Jakosky *et al.*, The Mars Atmosphere and Volatile Evolution (MAVEN) Mission. *Space Sci. Rev.* (2015). doi: 10.1007/s11214-015-0139-x
4. B. M. Jakosky, J. M. Grebowsky, J. G. Luhmann, D. A. Brain, Initial results from the MAVEN mission to Mars. *Geophys. Res. Lett.* 10.1002/2015GL065271 (2015).
5. S. Bougher *et al.*, Early MAVEN Deep Dip campaign reveals thermosphere and ionosphere variability. *Science* **350**, aad0459 (2015).
6. N. M. Schneider *et al.*, Discovery of diffuse aurora on Mars. *Science* **350**, aad0210 (2015).
7. L. Andersson *et al.*, Dust observations at orbital altitudes surrounding Mars. *Science* **350**, aad0398 (2015).
8. J. Gosling, The solar flare myth. *J. Geophys. Res.* **98**, 18937–18949 (1993). doi: 10.1029/93JA01896
9. J. E. P. Connerney *et al.*, The MAVEN magnetic field investigation. *Space Sci. Rev.* 10.1007/s11214-015-0169-4 (2015). doi: 10.1007/s11214-015-0169-4
10. J. S. Halekas *et al.*, The solar wind ion analyzer for MAVEN. *Space Sci. Rev.* 10.1007/s11214-013-0029-z (2013). doi: 10.1007/s11214-013-0029-z
11. D. H. Crider *et al.*, Mars Global Surveyor Observations of the Halloween 2003 solar Superstorm's Encounter with Mars. *J. Geophys. Res.* **110**, A09S21 (2005). doi: 10.1029/2004JA010881
12. D. L. Mitchell, C. Mazelle, J. P. McFadden, D. Larson, J. S. Halekas, J. E. P. Connerney, J. Espley, L. Andersson, J. G. Luhmann, R. J. Lillis, M. Fillingim, T. Hara, D. A. Brain, MAVEN observations of the Martian ionosphere and magneotheath [sic]. *Lunar Planet. Sci. Conf.*, abstract 3015, Houston, TX, 2015.
13. D. E. Larson, R. J. Lillis, P. A. Dunn, A. Rahmati, T. E. Cravens, K. Hatch, M. Robinson, D. Glaser, J. Chen, D. W. Curtis, C. Tiu, R. P. Lin, J. G. Luhmann, J. P. McFadden, J. Connerney, J. Halekas, B. M. Jakosky, The Solar Energetic Particle Experiment on MAVEN: First Results. *Lunar Planet. Sci. Conf.*, abstract 2890, Houston, TX, 2015.
14. F. Leblanc, J. G. Luhmann, R. Johnson, E. Chassefiere, Some expected impacts of a solar energetic particle event at Mars. *J. Geophys. Res.* **107**, 1058 (2002). doi: 10.1029/2001JA900178
15. S. W. Bougher, T. E. Cravens, J. Grebowsky, J. Luhmann, The aeronomy of Mars: Characterization by MAVEN of the upper atmospheric reservoir that regulates volatile escape. *Space Sci. Rev.* (2014). doi: 10.1007/s11214-014-0053-7

16. M. L. Mays *et al*., Ensemble modeling of CMEs using the WSA-ENLIL+Cone model. *Sol. Phys.* **290**, 1775–184 (2015). doi: 10.1007/s11207-015-0692-1
17. Y. Kamide, K. Kusano, No major solar flares but the largest geomagnetic storm in the present solar cycle. *Space Weather* **13**, 365–367 (2015). doi: 10.1002/2015SW001213
18. Y. Ma *et al*., Effects of crustal field rotation on the solar wind plasma interaction with Mars. *Geophys. Res. Lett.* **41**, 6563–6569 (2014). doi: 10.1002/2014GL060785
19. D. Vignes *et al*., The solar wind interaction with Mars: Locations and shapes of the bow shock and the magnetic pile-up boundary from the observations of the MAG/ER experiment onboard Mars Global Surveyor. *Geophys. Res. Lett.* **27**, 49–52 (2000). doi: 10.1029/1999GL010703
20. M. H. Acuña *et al*., Magnetic field and plasma observations at Mars: Initial results of the Mars Global Surveyor Mission. *Science* **279**, 1676–1680 (1998). doi: 10.1126/science.279.5357.1676; pmid: 9497279
21. C. T. Russell, R. C. Elphic, Observation of magnetic flux ropes in the Venus ionosphere. *Nature* **279**, 616–618 (1979). doi: 10.1038/279616a0
22. P. A. Cloutier *et al*., Venus-like interaction of the solar wind with Mars. *Geophys. Res. Lett.* **26**, 2685–2688 (1999). doi: 10.1029/1999GL900591
23. D. A. Brain *et al*., Episodic detachment of Martian crustal magnetic fields leading to bulk atmospheric plasma escape. *Geophys. Res. Lett.* **37**, L14108 (2010). doi: 10.1029/2010GL043916
24. T. Hara *et al*., The spatial structure of Martian magnetic flux ropes recovered by the Grad-Shafranov reconstruction technique. *J. Geophys. Res.* **119**, 1262–1271 (2014). doi: 10.1002/2013JA019414
25. W. E. McClintock *et al*., The Imaging Ultraviolet Spectrograph (IUVS) for the MAVEN Mission. *Space Sci. Rev.* 10.1007/s11214-014-0098-7 (2014). doi: 10.1007/s11214-014-0098-7
26. M. S. Chaffin *et al*., Three dimensional structure of the Mars H corona revealed by IUVS on MAVEN. *Geophys. Res. Lett.* 10.1002/2015GL065287 (2015).
27. C. Barth, A. I. Stewart, C. W. Hord, A. L. Lane, Mariner 9 ultraviolet spectrometer experiment: Mars airglow spectroscopy and variations in Lyman alpha. *Icarus* **17**, 457–468 (1972). doi: 10.1016/0019-1035(72)90011-5
28. J.-L. Bertaux *et al*., Discovery of an aurora on Mars. *Nature* **435**, 790–794 (2005). doi: 10.1038/nature03603; pmid: 15944698
29. S. Curry, M. Liemohn, X. Fang, Y. Ma, J. Espley, The influence of production mechanisms on pick-up ion loss at Mars. *J. Geophys. Res.* **118**, 554–569 (2013). doi: 10.1029/2012JA017665
30. J. P. McFadden, R. Livi, J. Luhmann, J. Connerney, D. Mitchell, C. Mazelle, L. Andersson, B. Jakosky, Structure of the martian ionosphere and atmospheric loss: MAVEN STATIC first results. *Lunar Planet. Sci. Conf.*, abstract 2899 (2015).
31. H. Nilsson *et al*., Birth of a comet magnetosphere: A spring of water ions. *Science* **347**, aaa0571 (2015). doi: 10.1126/science.aaa0571; pmid: 25613894
32. A. Rahmati *et al*., Pickup ion measurements by MAVEN: A diagnostic of photochemical oxygen escape from Mars. *Geophys. Res. Lett.* **41**, 4812–4818 (2014). doi: 10.1002/2014GL060289
33. S. Barabash, A. Fedorov, R. Lundin, J. A. Sauvaud, Martian atmospheric erosion rates. *Science* **315**, 501–503 (2007). doi: 10.1126/science.1134358; pmid: 17255508
34. E. Dubinin *et al*., Ion energization and escape on Mars and Venus. *Space Sci. Rev.* **162**, 173–211 (2011). doi: 10.1007/s11214-011-9831-7
35. Y. Futaana *et al*., Mars Express and Venus Express multi-point observations of geoeffective solar flare events in December 2006. *Planet. Space Sci.* **56**, 873–880 (2008). doi: 10.1016/j.pss.2007.10.014
36. D. Najib, A. F. Nagy, G. Tóth, Y. Ma, Three-dimensional, multifluid, high spatial resolution MHD model studies of the solar wind interaction with Mars. *J. Geophys. Res.* **116**, A05204 (2011). doi: 10.1029/2010JA016272
37. C. Dong *et al*., Solar wind interaction with the Mars upper atmosphere: Results from the one-way coupling between the multifluid MHD model and the MTGCM model. *Geophys. Res. Lett.* **41**, 2708–2715 (2014). doi: 10.1002/2014GL059515
38. E. Dubinin *et al*., Ionospheric storms on Mars: Impact of corotating interaction region. *Geophys. Res. Lett.* **36**, L01105 (2009). doi: 10.1029/2008GL036559
39. N. J. T. Edberg *et al*., Pumping out the atmosphere of Mars through solar wind pressure pulses. *Geophys. Res. Lett.* **37**, L03107 (2010). doi: 10.1029/2009GL041814
40. R. Ramstad *et al*., Phobos 2/ASPERA data revisited: Planetary ion escape rate from Mars near the 1989 solar maximum. *Geophys. Res. Lett.* **40**, 477–481 (2013). doi: 10.1002/grl.50149
41. R. Ramstad *et al*., The Martian atmospheric ion escape rate dependence on solar wind and solar EUV conditions: 1. Seven years of Mars Express observations. *J. Geophys. Res.* **120**, 1298–1309 (2015). doi: 10.1002/2015JE004816
42. H. Nilsson *et al*., Heavy ion escape from Mars, influence from solar wind conditions and crustal magnetic fields. *Icarus* **215**, 475–484 (2011). doi: 10.1016/j.icarus.2011.08.003
43. B. Wood, H.-R. Müller, G. P. Zank, J. L. Linsky, S. Redfield, New Mass-loss measurements from Astrospheric Ly-a absorption. *Astrophys. J.* **628**, L143–L146 (2005). doi: 10.1086/432716

ACKNOWLEDGMENTS

The results presented here represent the work of hundreds of scientists and engineers who designed, built, and operated the spacecraft and instruments and carried out the scientific analyses. We are indebted to them beyond words. The MAVEN mission has been funded by NASA through the Mars Exploration Program. Additional support was provided by CNES for the SWEA instrument and analysis, and by the Belgian American Educational Foundation. Part of this research was carried out at the Jet Propulsion Laboratory, California Institute of Technology, under a contract with the National Aeronautics and Space Administration. M. L. Mays and D. Odstrcil provided valuable analysis with the WSA-ENLIL+Cone model. Data from the MAVEN mission have been made available via the Planetary Data System (accessible via http://atmos.nmsu.edu/data_and_services/atmospheres_data/MAVEN/maven_main.html).

15 July 2015; accepted 18 September 2015
10.1126/science.aad0210

MAVEN observations of the response of Mars to an interplanetary coronal mass ejection

B. M. Jakosky *et al.*

Science **350**, (2015);
DOI: 10.1126/science.aad0210